ARTICLES

Journal of Semiconductors
(2022) 43, 124101
doi: 10.1088/1674-4926/43/12/124101

Humidity sensor based on BiOBr synthesized under ambient condition

Chaofan Cao[1, †], Guixian Xiao[1], and Yao Lu[2, †]

[1]Second Affiliated Hospital, Shenyang Medical College, Shenyang 110035, China

[2]State Key Laboratory of Automotive Safety and Energy, School of Vehicle and Mobility, Tsinghua University, Beijing 100084, China

Abstract: Flexible humidity sensors are effective portable devices for human respiratory monitoring. However, the current preparation of sensitive materials need harsh terms and the small production output limits their practicability. Here, we report a synthesis method of single-crystal BiOBr nanosheets under room temperature and atmospheric pressure based on a sonochemical strategy. A flexible humidity sensor enabled by BiOBr nanosheets deliver efficient sensing performance, a high humidity sensitivity (I_g/I_0 = 550%) with relative humidity from 40% to 100%, an excellent selectivity, and a detection response/recovery time of 11 and 6 s, respectively. The flexible humidity sensor shows a potential application value as a wearable monitoring device for respiratory disease prevention and health monitoring.

Key words: human breathing; BiOBr nanosheets; sonochemical strategy; flexible humidity sensor

Citation: C F Cao, G X Xiao, and Y Lu, Humidity sensor based on BiOBr synthesized under ambient condition[J]. *J. Semicond.*, 2022, 43(12), 124101. https://doi.org/10.1088/1674-4926/43/12/124101

1. Introduction

Breathing is a rhythmic activity of the human body, and its frequency and strength depend on the level of the body's activity. The main purpose of breathing is to provide oxygen to the body and remove carbon dioxide[1, 2]. The humidity, concentration, flow rate, and pressure of breathing are important indicators for disease diagnosis, treatment and prognosis evaluation, as well as pulmonary function projects in medicine and other fields[3–5]. Wearable devices such as wearable humidity sensors, can easily conform to and integrate with human skin, machines, and other curved surfaces, which enable rapid, continuous, and noninvasive capture of the breathing state[6–10].

At present, the research on flexible humidity sensors mainly focuses on resistive and capacitive types[11–15]. Among them, the resistive humidity sensors have widely been studied due to their simple fabrication and easy integration. The resistive humidity sensors display a resistance-change signal when the sensing material interacts with water molecules[13, 16]. Various moisture-sensitive materials have been explored to date, such as graphene oxide (GO)[17], carbon nanotubes[18], two-dimensional materials[19], and porous membranes[16]. For example, Xu *et al.*[20] reported a humidity sensor based on supramolecular graphene modified with sodium naphthalene-1-sulfonate and silver nanoparticles. Their sensor has a high sensitivity to humidity and a fast response and recovery time (⩽1 s). However, GO prepared by Hummer's method requires strong acid-corrosion resistance and a complex modification process, which greatly increases the cost and power consumption of the sensor. A recent humidity sensor based on a two-dimensional MoS_2 field-effect transistor requires a high gate operating voltage (80 V) and a complex preparation process; therefore, this sensor also increases the power consumption and incurs a high manufacturing cost[21]. Although these materials have interesting structural and electronic properties, high sensitivity, and fast response time, their production costs remain excessively high and the fabrication processes are complex. Therefore, high-performance humidity sensors fabricated from cheap materials through simple processes are in great demand.

BiOBr is one of the important bismuth oxide halide compounds. It is a ternary V–VI–VII semiconductor compound with tetragonal crystal structure. The layered structure of BiOBr is composed of tetragonal $[Bi_2O_2]^{2+}$ plates sandwiched between two Br ion plates. This inherent layered structure gives these materials fascinating optical, mechanical and electrical properties. At the same time, BiOBr can be prepared by various methods, such as hydrothermal[22], liquid-phase exfoliation[23], self-sacrifice template[24], which is considered to be an efficient material in a wide range of application. Here, we report a single-crystal BiOBr nanostructures synthesized using sonochemical methods under mild conditions. This method is simple and the reaction is completed at room temperature. Additionally, the synthesized BiOBr nanosheets have excellent humidity-sensing performance and ultrahigh selectivity. The fabricated humidity sensor based on BiOBr delivered a high humidity sensitivity (I_g/I_0 = 550%) from 40% to 100% RH and response/recovery time: 11 and 6 s, respectively, and showed an excellent humidity selectivity of BiOBr. The sensor can also detect the respiratory rate and gas volume of the human body. The prepared face masks have a large-scale application in the diagnosis of pulmonary function.

2. Methods

2.1. Materials

The raw materials of the pure metals bismuth (Bi, 99.99%, ⩾150 mesh) powder and hydrogen peroxide (H_2O_2,

Correspondence to: C F Cao, workchaofan@163.com; Y Lu, yaolu@mail.tsinghua.edu.cn

Received 30 JUNE 2022; Revised 25 JULY 2022.

©2022 Chinese Institute of Electronics

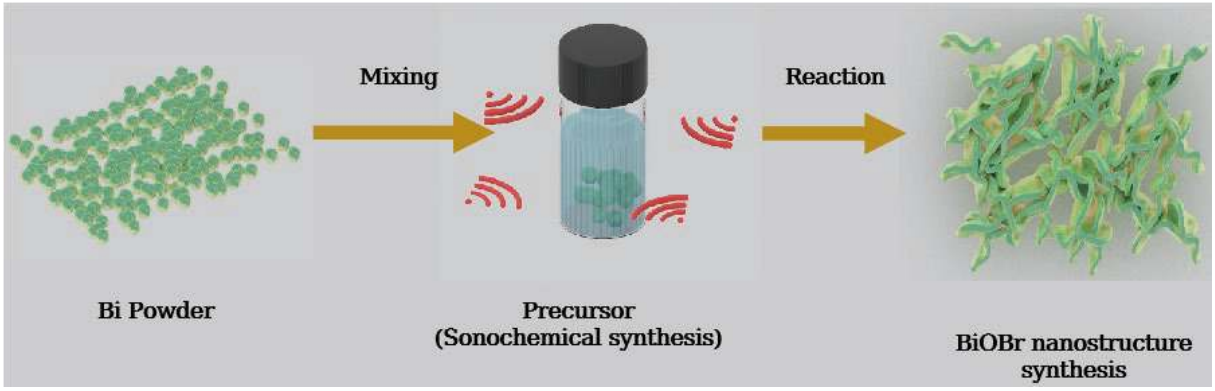

Fig. 1. (Color online) Schematic illustration on growing BiOBr nanostructures under ultrasonic treatment.

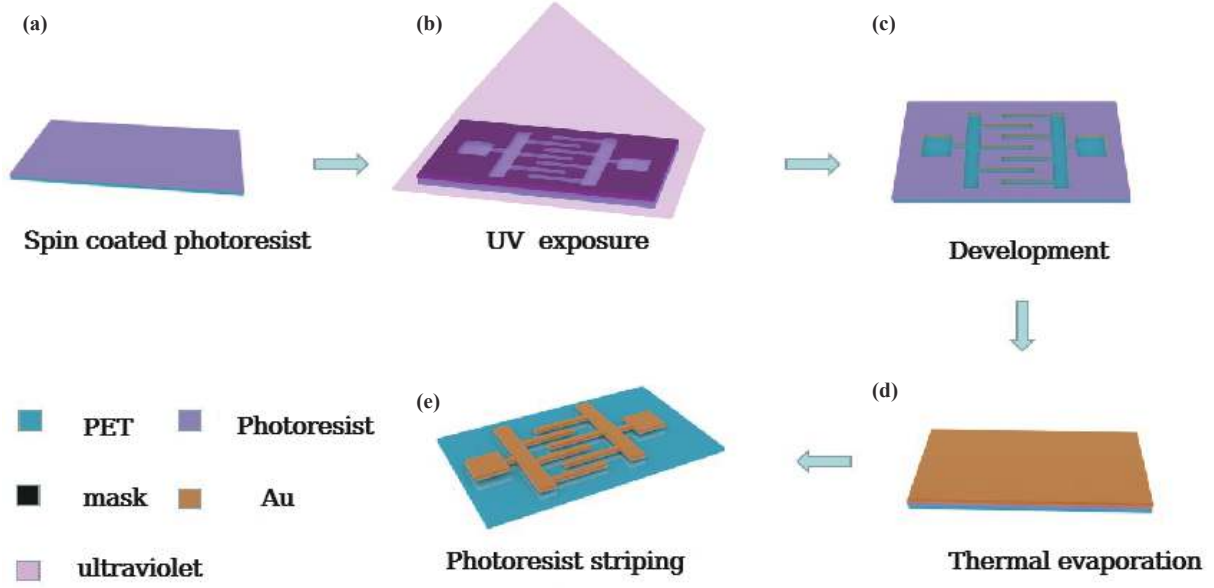

Fig. 2. (Color online) (a) Spin coating photoresist on PET substrate. (b) UV exposure under interdigital electrode patterned mask. (c) Develop the exposed PET substrate. (d) Thermal evaporation 60 nm Au electrode. (e) Acetone stripping to form interpolation gold electrode.

30%) are commercially available and were obtained from Sigma-Aldrich. The hydrobromic acid (HBr) was purchased from Sinopharm Chemical Reagent Co., Ltd. Home-made deionized water (DI H_2O) was used for all experiments.

2.2. Synthesis of BiOBr nanostructures

Fig. 1 shows the preparation of BiOBr nanostructures from the source material (Bi powder) via the sonochemical strategy under environmental conditions. In a typical experiment, 1 mmol Bi powder was added into the mixture solution with 5 mL H_2O_2 and 10 mL H_2O to form the suspension solution by stirring at a speed of 400 r/min. Then, 1 mL 1 M HBr was added into the suspension solution, and followed ultrasonic treatment at a frequency of 40 kHz for 2 h. The resultant products were collected by centrifugation and washed with H_2O for three times. Finally, the precipitate was dried under ambient conditions.

2.3. Preparation of the humidity sensor

A 60 nm Au interdigital pattern was first deposited on the PET substrate by photolithography and thermal evaporation, and a flexible interdigital electrode was prepared, as shown in Figs. 2(a)–2(e). The prepared BiOBr was then dispersed in ethanol solution by ultrasound, and the prepared BiOBr ethanol solution was spin coated on the electrode at 300 r/min. Finally, the equipment was baked on a hot plate at 80 °C for 10 min to add BiOBr materials and electrodes.

2.4. Microstructural characterizations

Powder X-ray diffraction (XRD, D8 Advance, Bruker, Germany) was utilized to evaluate the phase compositions under Cu Kα X-ray radiation (λ = 1.5406 Å). The microstructure and morphology of as-prepared samples were observed under a field emission scanning electron microscope (FESEM, S-4800, Hitachi, Japan) and high-resolution transmission electron microscopy (HRTEM, JEM-2100F, JEOL, Japan) equipped with energy dispersive X-ray spectroscopy (EDX, Quantax-STEM, Bruker, Germany). The compositions and valence band of the product were analyzed by X-ray photoelectron spectroscopy (XPS, Scientific K-Alpha, Thermo, USA), with a reference of C 1s peak at 284.6 eV. The photoluminescence was tested on a spectrometer (Fluromax-4P, Horiba Jobin Yvon, France) that was excited at 350 nm.

3. Results and discussion

3.1. BiOBr nanostructures

The successful preparation of BiOBr was characterized through SEM, X-ray diffraction, TEM, IR, and XPS. Panels a and b of Fig. 3 displays SEM images of the Bi powder and BiOBr

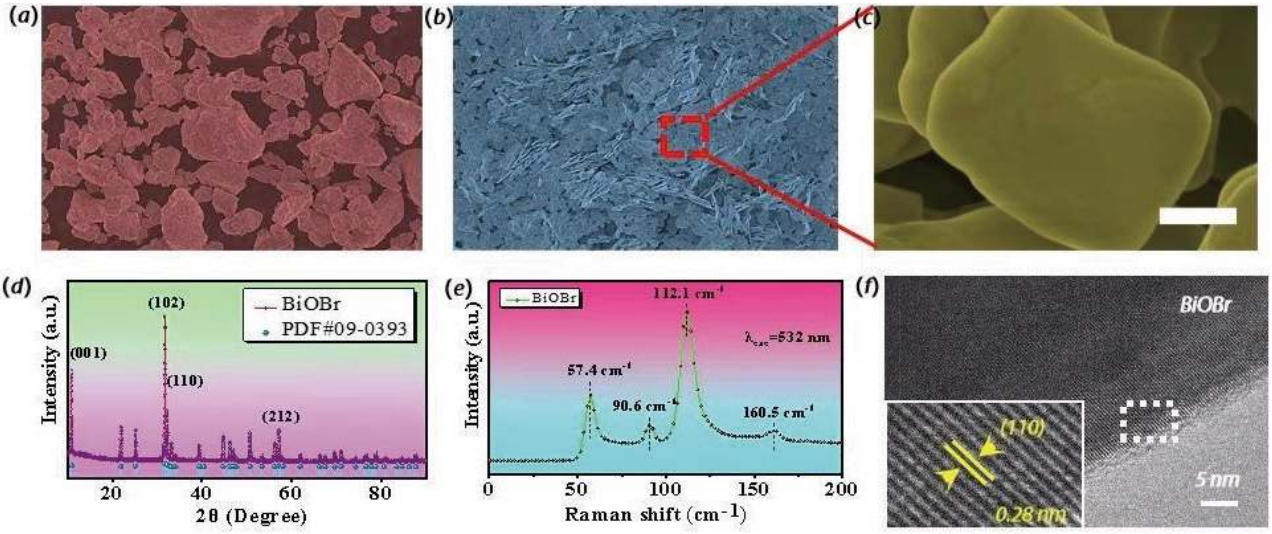

Fig. 3. (Color online) (a) SEM image of Bi powder. (b, c) SEM images of BiOBr nanostructure under different magnifications. (d) Typical XRD pattern of BiOBr nanostructure. (e) Raman spectrum of BiOBr nanostructure excited at 532 nm. (f) HRTEM images of BiOBr nanostructure, the down-left insets are the lattice fringes.

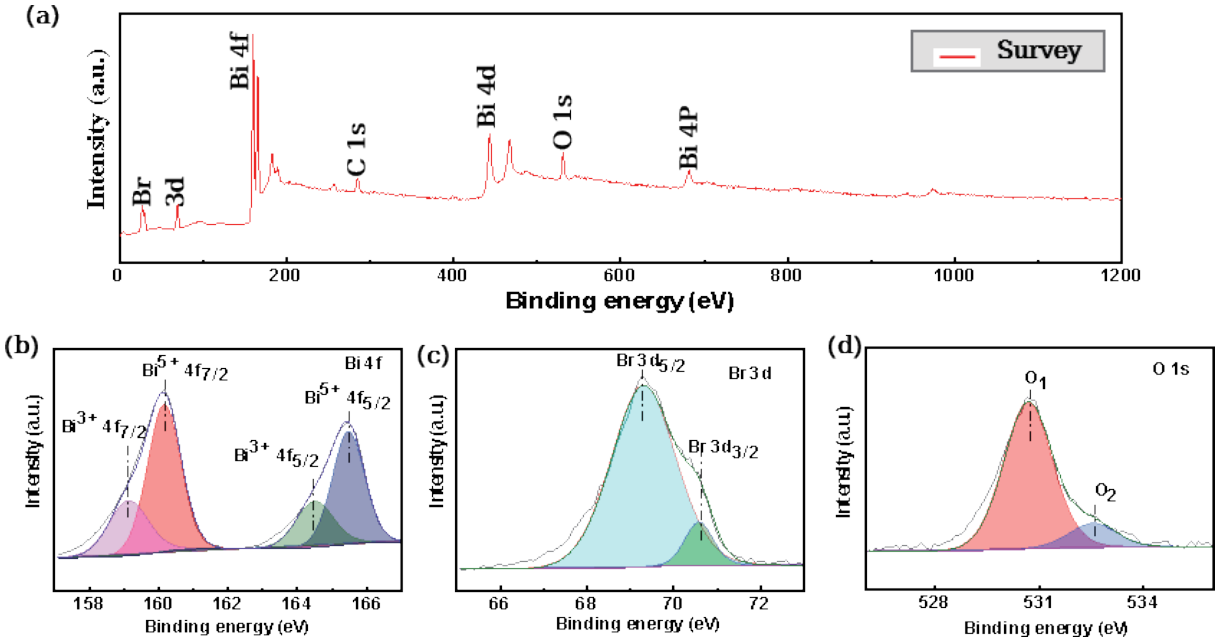

Fig. 4. (Color online) (a) XPS survey scan of BiOBr nanostructure. (b–d) High-resolution XPS spectra of Bi 4f, Br 3d and O 1s of BiOBr, respectively.

nanostructures, respectively. As shown in the images, the sonochemical strategy successfully incorporated the Bi powder into BiOBr nanosheets. After a statistical analysis of the particles in the SEM images, the approximate size range of the synthesized BiOBr nanostructures was determined as 0.5–1.5 μm (see Fig. 3(b), an enlarged view of Fig. 3(c)). The X-ray diffraction pattern of BiOBr (Fig. 3(d)) is consistent with JCPDS card No. 09-0393. The Raman spectrum of the BiOBr nanosheets is shown in Fig. 3(e). The spectral peaks at 57.4, 90.6, 112.1, and 160.5 cm^{-1} excited by 532 nm light were assigned to BiOBr. Furthermore, square nanostructures were observed in the TEM images. The HRTEM images (Fig. 3(f)) displayed clear lattice fringes with an interplanar spacing of 0.28 nm, corresponding to the (110) plane of BiOBr.

The elemental valence states and chemical compositions on the surfaces of the BiOBr nanosheets were analyzed using XPS. The measured XPS spectra (Fig. 4(a)) confirm the presence of only Bi, O, and Br elements in both samples. The peaks located at 159.1 and 164.4 eV in the Bi 3b spectrum of the BiOBr nanosheets (Fig. 4(b)) correspond to Bi 4f 5/2 and Bi 4f 7/2, respectively. Furthermore, the spin-orbit splitting energy between these two peaks is 5.3 eV, which indicates that normal Bi^{3+} resided on the nanosheet surfaces. However, the overall spectral distribution of the nanosheets shifted toward higher binding energies than those of pure Bi, indicating a high oxidation state of Bi in the nanosheets. According to previous studies, new peaks appear when the binding energies of 160.1 and 165.4 eV are raised by the higher valence of $Bi5^{+}$. The peaks at 69.2 and 70.6 eV in Fig. 4(c) correspond to Br $3d_{5/2}$ and Br $3d_{3/2}$, respectively. The O1s spectrum of the BiOBr sample (Fig. 4(d)) is broad and asymmetric and could be fitted to two peaks. The peaks appearing at high and low binding energies were assigned to surface-adsorbed oxygen and lattice oxygen components in the sample, respectively.

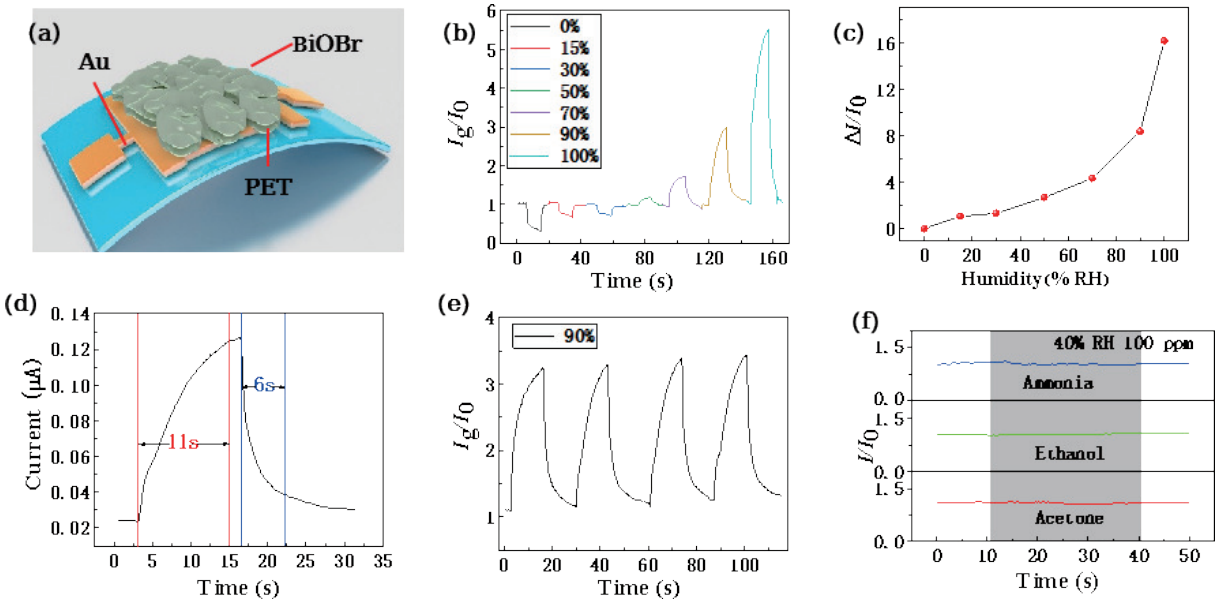

Fig. 5. (Color online) (a) Schematic illustration of a humidity sensor based on BiOBr nanostructure. (b) Time-dependent variation of relative current change of device under various concentrations of relative humidity. (c) Relative current change of sensor under different humidity relative to 0% humidity. (d) Response and recovery of the humidity sensor exposed to 90%. (e) Relative current changes of the humidity sensor under cyclic run between ambient humidity and 90% RH. (f) For the influence of other gases on the performance of humidity sensor, the relative humidity of the test environment is 40% RH, and the gas concentration is 100 ppm.

3.2. Humidity sensing properties

A BiOBr-based flexible humidity sensor was fabricated and its performance was characterized at 40% RH and 25 °C (Fig. 5(a)). Fig. 5(b) plots the sensitivities of the BiOBr humidity sensor as functions of time at different RH (0%–100%). The relative current of the sensor decreased over the humidity range 0%–30% and increased over the humidity range 50%–100% because our test was performed in an air environment with 40% RH. The humidity-dependent relative current variations of the sensor are clarified in Fig. 5(c). As the humidity increased from 0% to 100% RH, the relative current of the sensor increased to 1200%. This indicates that our sensor is highly sensitive to humidity.

In addition, the response and recovery time are important parameters of a humidity sensor in practical applications such as respiratory monitoring. In this work, we measured the time required for the sensor to reach equilibrium (95% of the maximum change) between 40% and 90% RH. During the measurement, the resistance change was measured while alternately moving the sensor between two humidity environments. The response and recovery time of the sensor were 10 and 6 s, respectively (Fig. 5(d)). We also characterized the cyclic stability of the device (Fig. 5(e)). When the humidity changed repeatedly between 40% and 90% RH, the response signal of the sensor fluctuated only slightly, indicating strong cycle performance and stability. Moreover, during respiration detection, the humidity sensor is directly interfered with by gas, so high selectivity for humidity is essential. The electrical response of the humidity sensor in the atmosphere of ethanol, acetone and ammonia gas. During the test, the relative humidity of the environment is controlled to be 40% and the gas concentration is 100 ppm. The test results are shown in Fig. 5(f). It can be seen that when the humidity sensor works at room temperature, its relative current basically does not change in the presence of ethanol, acetone, and ammonia. This indicates that the humidity sensor can be used as a highly selective humidity sensor.

3.3. Breathing monitoring

Given the excellent humidity performance and fast response time of the humidity sensor, we incorporated the sensor into an intelligent mask that detects human respiration in real time. As shown in Figs. 6(a) and 6(b), our smart mask is composed of sensors installed in a breathing valve. When the mask is worn, the user's breathing is detected in a relatively closed space. As the current of the sensor increases or decreases with each breath, we can monitor the changing intensity and frequency of the respiration by monitoring the magnitude and number of peaks, respectively. Fig. 6(c) compares the relative current changes of the sensor during deep and normal breathing. The intensity was much higher during deep breathing than during normal breathing. This implies that the sensor can detect the vital capacity. Additionally, the current of the smart mask increased and decreased in synchrony with the breathing pattern, so the changes in respiratory rate can be monitored through the number of peaks. As shown in Figs. 6(d)–6(f), our smart mask can monitor breathing at different frequencies (slow, normal, and fast) in real time. These results show that our intelligent mask can measure the respiratory status of the human body and help medical diagnoses of lung disease.

4. Conclusion

We have developed a high-performance flexible humidity sensor that is based on a sensitive material composed of BiOBr single-crystal biological nanostructured nanosheets. The material is prepared using a simple, low-cost sonochemical method suitable for large-scale production and demonstrates excellent humidity properties, with a humidity sensitivity of 550% (I_g/I_0) from 40% to 100% RH, response and recovery time 11 and 6 s, respectively, and excellent selectivity for

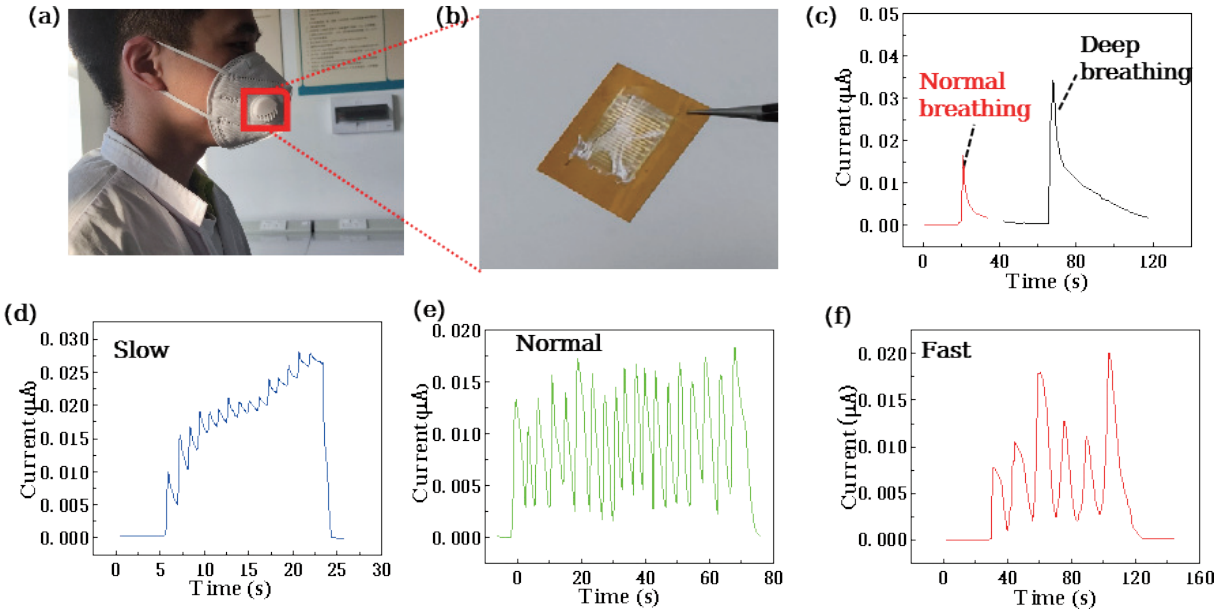

Fig. 6. (Color online) (a) The application of a humidity sensor in human respiratory monitoring is intelligent mask. (b) Photos of humidity sensors. (c) Response of the sensor under various breathing modes. (d–f) The smart mask's response under different breathing rates.

humidity. In experimental demonstrations, the sensor successfully detected human respiration patterns. This cost-effective flexible humidity sensor has potential applications in the diagnosis and treatment of respiratory diseases; for instance, as a wearable respiratory monitoring device for infection reduction and health monitoring.

Acknowledgements

The authors sincerely acknowledge financial support from the China Postdoctoral Science Foundation (No. 2021M691729), National Key R&D Program of China (No. 2021YFB2401901), Tsinghua-Toyota Joint Research Fund (No. 20213930025).

References

[1] Rolfe S. The importance of respiratory rate monitoring. Brit J Nurs, 2019, 28(8), 504

[2] Jonkman A H, De Vries H J, Heunks L M A. Physiology of the respiratory drive in ICU patients: implications for diagnosis and treatment. Crit Care, 2020, 24(1), 1

[3] Bigatello L, Pesenti A. Respiratory physiology for the anesthesiologist. Anesthesiology, 2019, 130(6), 1064

[4] McCafferty J. Respiratory heat and moisture loss in health, asthma and chronic obstructive pulmonary disease (COPD). University of Edinburgh, 2006

[5] Sylvester K P, Youngs L, Rutter M A, et al. Early respiratory diagnosis: benefits of enhanced lung function assessment. BMJ Open Respir Res, 2021, 8(1), e001012

[6] Baldo T A, de Lima L F, Mendes L F, et al. Wearable and biodegradable sensors for clinical and environmental applications. ACS Appl Electron Mater, 2020, 3(1), 68

[7] Lu Y, Xu K, Zhang L, et al. Multimodal plant healthcare flexible sensor system. ACS Nano, 2020, 14(9), 10966

[8] Li B, Xiao G, Liu F, et al. A flexible humidity sensor based on silk fabrics for human respiration monitoring. J Mater Chem C, 2018, 6(16), 4549

[9] Peng B, Zhao F, Ping J, et al. Recent Advances in nanomaterial - enabled wearable sensors: Material synthesis, sensor design, and personal health monitoring. Small, 2020, 16(44), 2002681

[10] Leng X, Wang Y, Wang F. Alcohols assisted hydrothermal synthesis of defect-rich MoS_2 and their applications in humidity sensing. Adv Mater Interfaces, 2019, 6(11), 1900010

[11] Al-Sehemi A G, Al-Assiri M S, Kalam A, et al. Sensing performance optimization by tuning surface morphology of organic (D-π-A) dye based humidity sensor. Sens Actuators B, 2016, 231, 30

[12] Lu Y, Xu K, Yang M Q, et al. Highly stable Pd/HNb_3O_8-based flexible humidity sensor for perdurable wireless wearable applications. Nanoscale Horiz, 2021, 6(3), 260

[13] Wang Y F, Sekine T, Takeda Y, et al. Fully printed PEDOT: PSS-based temperature sensor with high humidity stability for wireless healthcare monitoring. Sci Rep, 2020, 10(1), 1

[14] Bae Y M, Lee Y H, Kim H S, et al. Polyimide-polyurethane/urea block copolymers for highly sensitive humidity sensor with low hysteresis. J Appl Polym Sci, 2017, 134(24), 44973

[15] Farahani H, Wagiran R, Hamidon M N. Humidity sensors principle, mechanism, and fabrication technologies: a comprehensive review. Sensors, 2014, 14(5), 7881

[16] An H, Habib T, Shah S, et al. Water sorption in MXene/polyelectrolyte multilayers for ultrafast humidity sensing. ACS Appl Nano Mater, 2019, 2(2), 948

[17] Leng X, Luo D, Xu Z, et al. Modified graphene oxide/Nafion composite humidity sensor and its linear response to the relative humidity. Sens Actuators B, 2018, 257, 372

[18] Zhu P, Liu Y, Fang Z, et al. Flexible and highly sensitive humidity sensor based on cellulose nanofibers and carbon nanotube composite film. Langmuir, 2019, 35(14), 4834

[19] Yang J, Shi R, Lou Z, et al. Flexible smart noncontact control systems with ultrasensitive humidity sensors. Small, 2019, 15(38), 1902801

[20] Wang S, Chen Z, Umar A, et al. Supramolecularly modified graphene for ultrafast responsive and highly stable humidity sensor. J Phys Chem C, 2015, 119(51), 28640

[21] Zhao J, Li N, Yu H, et al. Highly sensitive MoS_2 humidity sensors array for noncontact sensation. Adv Mater, 2017, 29(34), 1702076

[22] Vadivel S, Vanitha M, Muthukrishnaraj A, et al. Graphene oxide–BiOBr composite material as highly efficient photocatalyst for degradation of methylene blue and rhodamine-B dyes. J Water Proc Eng, 2014, 1, 17

[23] Yu H, Huang H, Xu K, et al. Liquid-phase exfoliation into monolayered BiOBr nanosheets for photocatalytic oxidation and reduction. ACS Sustaine Chem Eng, 2017, 5(11), 10499

[24] Peng Y, Xu J, Liu T, et al. Controlled synthesis of one-dimensional BiOBr with exposed (110) facets and enhanced photocatalytic activity. CrystEngComm, 2017, 19(43), 6473

Chaofan Cao got his M.S degree in 2018 at China Medical University. Then he joined the Respiratory Department of the Second Affiliated Hospital of Shenyang Medical College as an attending physician. His research interests include chronic airway disease, lung function, and respiratory endoscopy.

Guixian Xiao graduated from the Medical School of Tongji University in 1989. Head of respiratory Department of the Second Affiliated Hospital of Shenyang Medical College. Her research interests include bronchial asthma and chronic obstructive pulmonary disease.

Yao Lu got his M.S and Ph.D. degree in 2020 at the University of Science and Technology Beijing. Then he joined the State Key Laboratory of Automotive Safety and Energy at Tsinghua University as an assistant research fellow. His research interests include smart lithium-ion batteries and smart cell sensors.